The Astrophysical Journal, 774:86 (14pp), 2013 September 1 doi:10.1088/0004-637X/774/1/86

MASSIVE CLUMPS IN LOCAL GALAXIES: COMPARISONS WITH HIGH-REDSHIFT CLUMPS

Bruce G. Elmegreen[1], Debra Meloy Elmegreen[2], J. Sánchez Almeida[3], C. Muñoz-Tuñón[3], J. Dewberry[2], J. Putko[2,4], Y. Teich[2], and M. Popinchalk[2,5]
[1] IBM Research Division, T. J. Watson Research Center, Yorktown Hts., NY 10598, USA
[2] Vassar College, Dept. of Physics and Astronomy, Poughkeepsie, NY 12604, USA
[3] Instituto de Astrof'sica de Canarias, C/via Láctea, s/n, E-38205, La Laguna, Tenerife, Spain
[4] Middlebury College, Dept. of Physics, Middlebury, VT 05753, USA
[5] Wesleyan University, Dept. of Astronomy, Middletown, CT 06459, USA
Received 2013 May 7; accepted 2013 July 17; published 2013 August 19

ABSTRACT

Local UV-bright galaxies in the Kiso survey include clumpy systems with kiloparsec-size star complexes that resemble clumpy young galaxies in surveys at high redshift. We compare clump masses and underlying disks in several dozen galaxies from each of these surveys to the star complexes and disks of normal spirals. Photometry and spectroscopy for the Kiso and spiral sample come from the Sloan Digital Sky Survey. We find that the largest Kiso clumpy galaxies resemble Ultra Deep Field (UDF) clumpies in terms of the star formation rates, clump masses, and clump surface densities. Clump masses and surface densities in normal spirals are smaller. If the clump masses are proportional to the turbulent Jeans mass in the interstellar medium, then for the most luminous galaxies in the sequence of normal:Kiso:UDF, the turbulent speeds and surface densities increase in the proportions 1.0:4.7:5.0 and 1.0:4.0:5.1, respectively, for fixed restframe *B*-band absolute magnitude. For the least luminous galaxies in the overlapping magnitude range, the turbulent speed and surface density trends are 1.0:2.7:7.4 and 1.0:1.4:3.0, respectively. We also find that while all three types have radially decreasing disk intensities when measured with ellipse-fit azimuthal averages, the average profiles are more irregular for UDF clumpies (which are viewed in their restframe UV) than for Kiso galaxies (viewed at *g*-band), and major axis intensity scans are even more irregular for the UDF than Kiso galaxies. Local clumpy galaxies in the Kiso survey appear to be intermediate between UDF clumpies and normal spirals.

Key words: galaxies: evolution – galaxies: peculiar – galaxies: starburst – galaxies: star formation – ISM: kinematics and dynamics – stars: formation

Online-only material: color figures

1. INTRODUCTION

Disk galaxies at increasing redshift become more irregular (Abraham et al. 1996; Conselice et al. 2005) and clumpy (Elmegreen et al. 2004; see review in Shapley 2011) as a result of an increased frequency of mergers in the denser universe (Kartaltepe et al. 2012; Puech et al. 2012; Kaviraj et al. 2013; McLure et al. 2013), and because of higher gas fractions (Tacconi et al. 2013; Bothwell et al. 2013) and velocity dispersions (Law et al. 2009; Förster Schreiber et al. 2009; Newman et al. 2013) that lead to more violent gravitational instabilities (Elmegreen & Elmegreen 2005; Bournaud et al. 2007; Genzel et al. 2008; Ceverino et al. 2010; Wisnioski et al. 2011). Over time, mergers become less frequent, and an increasing stellar mass fraction gives a galaxy more stability, with density waves in the stars replacing violent clump formation in the gas (Cacciato et al. 2012).

Local galaxies with relatively large star-forming complexes are nearby analogs of high redshift clumpy galaxies that allow a comparison of large-scale star forming regions over time. For example, local dwarf irregulars resemble high redshift galaxies with respect to gas fraction, relative clump size, and relative thickness (Elmegreen et al. 2009b). Local tadpole galaxies (Elmegreen et al. 2012), which include the sub-class iI,c (Noeske et al. 2000) of blue compact dwarfs (BCDs; see also Gil de Paz et al. 2003; Kniazev et al. 2001) and a high fraction of extremely metal-poor BCDs (Papaderos et al. 2008; Morales-Luis et al. 2011), resemble high-redshift tadpoles, which account for 10% of large galaxies in the Hubble Ultra Deep Field (UDF; Elmegreen et al. 2007, 2012). Tadpoles contain one giant clump of stellar mass $M_* \sim 10^7\,M_\odot$ (Elmegreen et al. 2012) with a tail to the side. The clumps in several local tadpoles have lower metallicities than the rest of the galaxy, suggestive of accretion (Sánchez Almeida et al. 2013). Similar localized metallicity drops are observed in $M_* \sim 10^{10}\,M_\odot$ star-forming galaxies at high redshift (e.g., Cresci et al. 2010; Queyrel et al. 2012). Some BCDs suggest active accretion as well, considering the irregular and sometimes non-rotating pools of H I gas that surround them (Brinks & Klein 1988; Taylor et al. 1996; Thuan & Izotov 1997; van Zee et al. 1998a, 1998b; Putman et al. 1998; Wilcots & Miller 1998; Pustilnik et al. 2001; Hoffman et al. 2003),

Luminous blue compact galaxies are another type of local analog that are small, clumpy, and irregular with high gas fractions ($\gtrsim$10%) and distorted kinematics (Garland et al. 2007). They are locally rare, possibly interacting (Garland et al. 2004), and like intermediate-redshift ($z \sim 0.5$) blue compact galaxies (Hoyos et al. 2007), they may evolve into dwarf ellipticals or low-mass irregulars with dynamical masses of 10^{10}–$10^{11}\,M_\odot$.

Other local analogs of high-redshift galaxies have higher masses than BCDs or luminous blue compact galaxies. Casini & Heidmann (1976) studied the massive clumpy irregular galaxies Markarian 7, 8, 296, and 325, in a survey of Markarian galaxy pairs. With considerable foresight, they suggested that the clumps could be galaxy fragments and that the galaxies might settle down to normal Hubble types over time. Heidmann (1987) summarized this rare type of galaxy noting that the clumps have 100 times the luminosity of 30 Doradus (Benvenuti et al. 1982) and $\sim 10^8\,M_\odot$ of ionized gas; Mrk 325 has X-ray

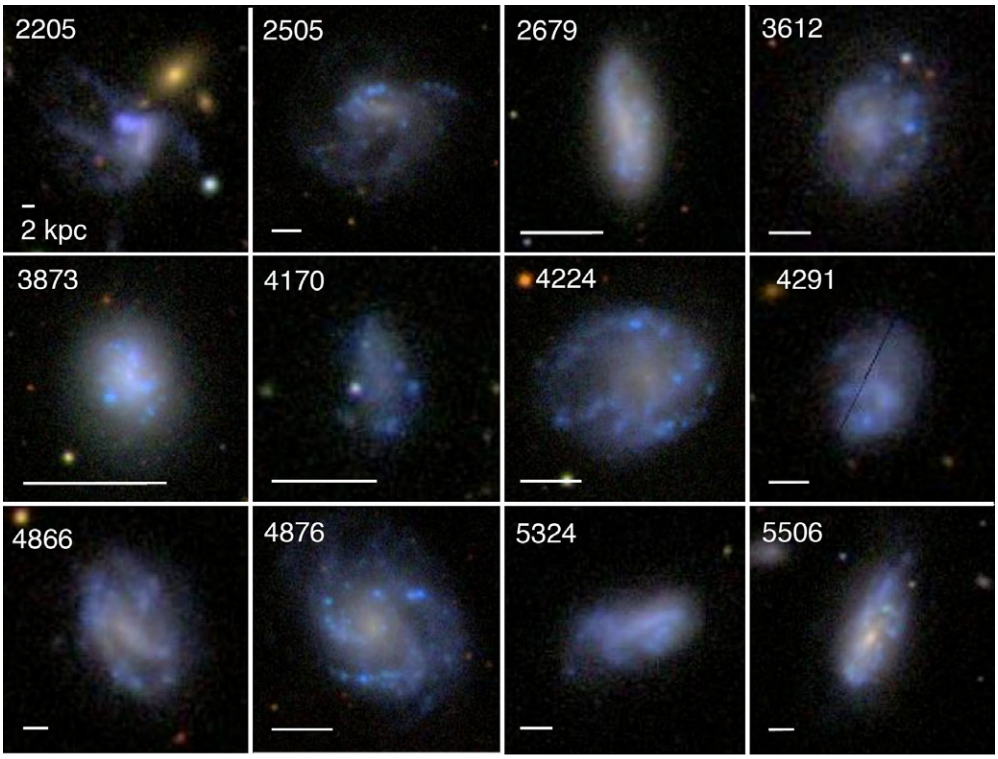

Figure 1. Kiso galaxies with Kiso numbers indicated and scale bars equal to 2 kpc. Color images are from the SDSS in *g*, *r*, and *i* passbands.
(A color version of this figure is available in the online journal.)

emission equivalent to 10^4 supernovae remnants. In Mrk 296, there are several large clumps along a jagged line, making it look like a crooked chain galaxy; the share of the total stellar mass in each clump is $\sim 10^8\ M_\odot$ (Casini et al. 1979). Three other massive clumpy galaxies were subsequently studied from the Kiso Ultraviolet Galaxy survey by Maehara et al. (1988): 1618+378, 1624+404, 1626+413, to which a fourth was added, Mrk 297. In terms of clump mass, these galaxies resemble high-redshift clumpy galaxies. Maehara et al. (1988) state that they are ~10 times brighter and ~3 times larger than classic irregulars, and the most distant ones are at 120 Mpc.

Local ultraviolet luminous galaxies also resemble star-forming galaxies at $z > 1$ (Heckman et al. 2005). The most compact of these are brighter in the UV than local BCDs, having $M_* \sim 10^{10}\ M_\odot$, and resemble Lyman break galaxies in luminosity, mass, metallicity, and star formation rate (Hoopes et al. 2007). Lyman break analogs like this also compare well morphologically to clumpy high redshift galaxies (Overzier et al. 2008, 2009, 2010). Similar studies by Hibbard & Vacca (1997), Barden et al. (2008), Petty et al. (2009), and others show significant loss of faint, small, and peripheral structures in local starburst galaxies when viewed as if they were at high redshift, so that only the most clumpy and irregular of the nearby systems, many of which are interacting, resemble young galaxies. Petty et al. (2009) suggest that Mrk 8, studied also by Casini & Heidmann (1976), NGC 3079, and NGC 7673 resemble clumpy star-forming galaxies in the $z = 1.5$–4 range.

Here we study low-redshift clumpy galaxies from the Kiso Survey for Ultraviolet-Excess Galaxies (Miyauchi-Isobe et al. 2010). This is a survey of $\sim 10^4$ galaxies brighter than 18th magnitude (photographic) covering 7000 deg^2 made with the Kiso Schmidt telescope. The survey classified uv-bright galaxies according to various morphologies using the Palomar Observatory Sky Survey and the Sloan Digital Sky Survey (SDSS; Stoughton et al. 2002). We are interested in classification type Ic, which has large blue clumps, and type Ig, which has a single large clump. The survey contains 176 Ic and 83 Ig galaxies, of which 158 of the 259 total are in the SDSS. Many of these 158 galaxies are spirals with one or more bright star-forming regions. Others are irregulars or possible interactions; 95 have SDSS-DR7 spectra (Abazajian et al. 2009). A sample of 36 of those with spectra were chosen for the present study, based on their low inclination, relative isolation, and clumpiness.

In Section 2, we measure the magnitudes in five SDSS filters of each prominent clump in the Kiso sample and determine the masses, ages, and extinctions in these clumps from population synthesis models. In Section 3, we also determine the galaxy star formation rates from the SDSS single-fiber spectra. The Kiso clumps are compared with star-forming clumps in 20 representative local spiral galaxies covering a range of Hubble types and arm classes. These results are then compared with the properties of clumps in high-redshift clumpy galaxies of the "clump-cluster" type (Elmegreen et al. 2005b). Radial light profiles are also compared in the different galaxy samples in Section 4. A discussion is in Section 5, and conclusions are in Section 6.

2. STAR-FORMING CLUMPS

2.1. Photometry and Modeling

Archival images of 36 clumpy UV-bright galaxies in the Kiso survey were obtained in u, g, r, i, z filters from the SDSS survey Web site (http://www.sdss.org), as listed in Table 1 and shown in Figures 1–3. The Kiso Ultraviolet Galaxy (KUG) numbers in Table 1 come from the Kiso2000 catalog[6] (Miyauchi-Isobe et al. 2010); we also give the Kiso number, which is the catalog

[6] http://vizier.cfa.harvard.edu (KUG2000)

Table 1
Kiso Galaxies

KUG	Kiso	Other	Type	Features	Distance (Mpc)	M_B (mag)
KUG 0726+400	2205		Ic	streamer	205.6	−20.14
KUG 0757+373	2505	UGC 04157	Ic	off-center	53.9	−17.73
KUG 0813+243	2679	IC2556	Ic		29.3	−17.35
KUG 0926+455	3612		Ic	spiral	59.1	−17.60
KUG 0937+485	3873	Mrk 1418, UGC 05151	Ic		11.0	−15.91
KUG 0950+295	4170		Ic		21.6	−14.10
KUG 0952+335	4224	UGC 05326	Ic	off-center	19.0	−16.80
KUG 0956+439B	4291		Ic		69.9	−17.23
KUG 1045+334	4866		Ic	off-center	91.6	−18.91
KUG 1046+330	4876	IC 2604, UGC 05927, VV 538	Ic	spiral	22.1	−17.27
KUG 1125+240	5324		Ig	bar	80.5	−19.09
KUG 1131+159	5506		Ig	streamer	70.2	−19.33
KUG 1140+331	5678		Ic		135.4	−18.58
Irr KUG 1145+130	5781	near IC 0737	Ic		48.8	−17.21
KUG 1150+353	5886		Ic	spiral	87.6	−19.71
KUG 1155+281	5979	NGC 4004, VV 230, Mrk 0432	Ic	streamer	45.9	−19.06
KUG 1204+248	6164		Ic	spiral	105.7	−19.10
KUG 1218+179	6487		Ig	BCD	28.3	−17.12
KUG 1226+206	6630		Ic	off-center spiral	94.5	−18.94
I KUG 1229+207	6667		Ic	spiral	26.0	−16.64
KUG 1229+250	6678	IC 3472	Ic	spiral	94.9	−18.02
KUG 1251+363	6971		Ic	streamer	58.0	−17.51
KUG 1256+274	7029	Mrk 0057	Ic	streamer	105.1	−19.47
KUG 1308+368	7167	NGC 5002, UGC 08254	Ic	bar	15.6	−16.08
KUG 1310+230	7186	NGC 5012A	Ic	off-center, bar, spiral	35.4	−18.02
KUG 1319+356	7256		Ic	off-center	80.7	−18.92
KUG 1336+312	7400		Ic	spiral?	65.9	−17.99
KUG 1408+163	7878		Ic	off-center	32.3	−17.32
KUG 1409+110	7914		Ic	bar	102.2	−18.57
KUG 1425+137	8109	UGC 09273	Ic		18.0	−15.66
KUG 1426+234	8116	NGC 5637	Ic	spiral	72.6	−19.90
KUG 1427+262	8123		Ic	spiral?	67.2	−18.05
KUG 1603+206	8491	Mrk0297, NGC 6052, Arp 209, VV 0862	Ic		66.3	−20.14
KUG 1619+408	8664		Ic	spiral	297.5	−20.69
KUG 1624+404	8708	Mrk 881	Ic		120.5	−20.22
KUG 2316+154	9363		Ic	off-center	63.2	−17.51

entry number minus 1. Although the galaxies in this sample were selected because of their bright star-forming clumps, there are many distinct morphologies. Some, like Kiso 8491, are dominated by many large blue clumps in an irregular pattern. Others, like Kiso 5886, have regular spiral arms with big clumps in the arms. Kiso 2205 and 6971 are irregularly shaped with long streamers; Kiso 5979 has a long arm that looks tidal in origin; Kiso 7186, 7256, and 7878 have off-center bulges; Kiso 5324 and 7914 show central bars, and 7186 has an offset bar. Kiso 4170 is totally irregular. Most of the Kiso galaxies studied here have a red central region that is displaced from the center of the outer isophotes. These features are noted in the table, along with the Kiso Ic or Ig type, the distance in Mpc from the NASA/IPAC Extragalactic Database (NED), and the absolute blue magnitude (from NED).

The primary selection criterion for the measured galaxies, aside from the requirement of a low inclination for visibility of the disks and a relative isolation to remove obvious mergers, was the presence of large star-forming complexes. Examination of the images shows many other odd features, however, as detailed in the previous paragraph. The few with off-center bulges or bars are interesting because these asymmetries suggest a short-lived phase or an unusual dynamical process, either of which may lead to heightened gas turbulence. General disk irregularities suggestive of pervasive and massive gravitational instabilities may also lead to heightened turbulence. Such turbulence should increase the Jeans length in the disk, making the largest star-forming complexes larger than normal. We discuss the Jeans length and mass more in Section 2.2.1, where we use the observed clump properties to suggest an increase in turbulent speed.

A representative sample of 20 nearby spirals in SDSS was selected from our previous study of arm properties (Elmegreen et al. 2011) based on infrared images from the *Spitzer* Survey of Stellar Structure in Galaxies, S^{4}G (Sheth et al. 2010). These galaxies are listed in Table 2 along with their Hubble type (from NED), Arm Class (Elmegreen & Elmegreen 1987), and absolute blue magnitude (from NED). They were chosen to cover the same range of absolute B-band magnitude as the Kiso galaxies, but were not matched to star formation rate or selected for any particular morphology. They span Hubble types Sb through Sm and include flocculent, multiple arm, and grand design spirals. They are a good comparison sample for examining star-forming complexes since the Kiso galaxies are intensely starbursting and these spirals are not.

Photometric measurements on sky-subtracted and aligned images for both the Kiso galaxies and the local spirals were performed with IRAF (Image Reduction and Analysis Facility)

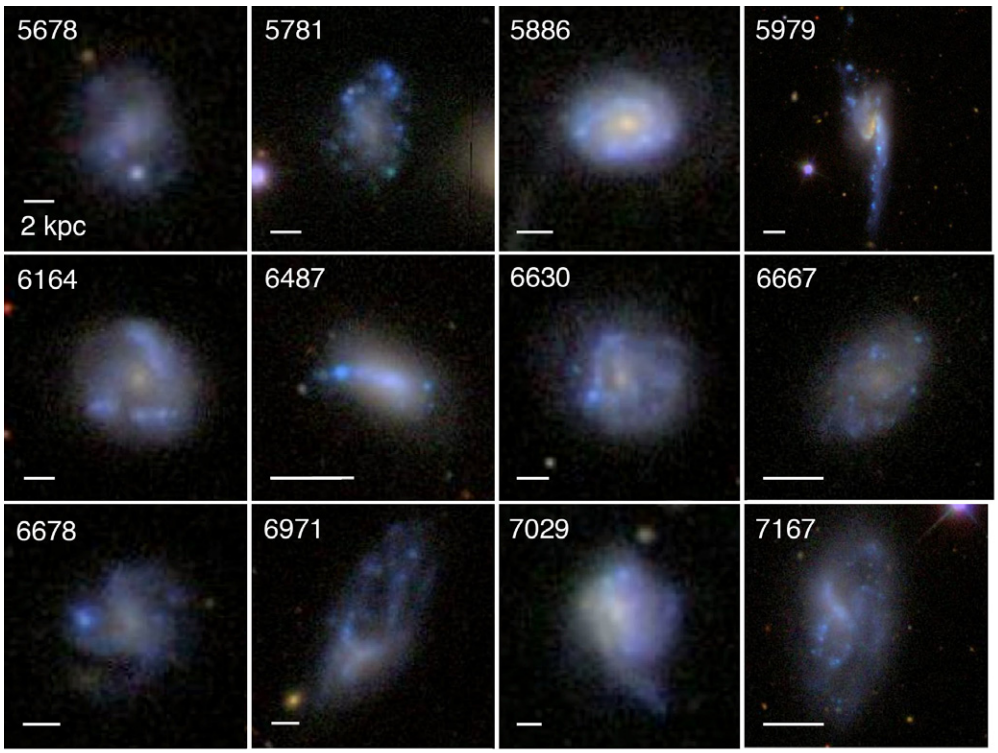

Figure 2. Continues from Figure 1; Kiso galaxies with Kiso numbers indicated and scale bars equal to 2 kpc. Color images are from the SDSS in *g*, *r*, and *i* passbands. (A color version of this figure is available in the online journal.)

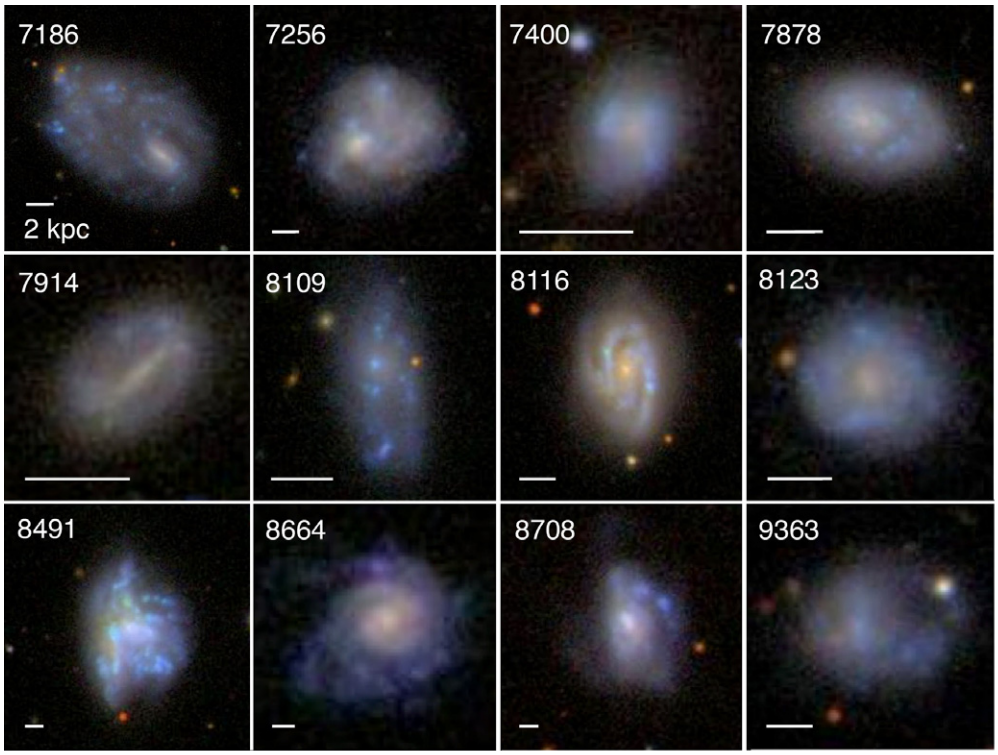

Figure 3. Continues from Figure 2; Kiso galaxies with Kiso numbers indicated and scale bars equal to 2 kpc. Color images are from the SDSS in *g*, *r*, and *i* passbands. (A color version of this figure is available in the online journal.)

to determine the masses, ages, and extinctions of the clumps. The largest clumps were identified by eye on *g*-band SDSS images, and their magnitudes were measured with circular apertures in the *apphot* task, which subtracts the local background from an annulus surrounding the aperture. The masses, surface densities, ages, and extinctions of the clumps were estimated from this photometry by fitting the data to models in Bruzual & Charlot (2003) that assume a Chabrier initial mass function and solar metallicity (models with 0.4 times the solar metallicity had negligible differences compared to the clump-to-clump scatter).

Table 2
SDSS Local Spiral Galaxies

NGC	Type	Arm Class	Distance (Mpc)	M_B (mag)
1087	SAB(rs)c	flocculent	20.80	−20.63
2903	SAB(rs)bc	grand design	6.52	−19.96
3184	SAB(rs)cd	multiple arm	8.17	−19.22
3344	(R)SAB(r)bc	multiple arm	7.21	−18.79
3351	SB(r)b	grand design	9.30	−19.58
3433	SA(s)c	grand design	35.80	−20.61
3596	SAB(rs)c	flocculent	15.20	−19.22
4254	SA(s)c	multiple arm	32.30	−22.44
4303	SAB(rs)bc	multiple arm	20.30	−21.42
4449	IBm	...	3.55	−17.81
4519	SB(rs)d	flocculent	15.80	−18.84
4535	SAB(s)c	grand design	26.00	−21.76
4618	SB(rs)m	flocculent	8.12	−18.42
5055	SA(rs)bc	flocculent	7.54	−20.36
5194	SA(s)bc	grand design	7.54	−20.72
5248	SAB(rs)bc	grand design	15.40	−20.31
5371	SAB(rs)bc	grand design	36.20	−21.62
5457	SAB(rs)cd	multiple arm	4.94	−20.26
5474	SA(s)cd pec	flocculent	5.36	−17.35
5584	SAB(rs)cd	multiple arm	22.10	−20.02

Table 3
UDF Clumpy Galaxies

UDF	Redshift	M_B (mag)
533	2.42	−19.43
1666	1.35	−20.64
1681	0.12	−12.54
1775	2.15	−18.97
2012	2.98	−22.10
2340	1.32	−18.30
2350	3.09	−19.73
2499	0.69	−15.38
2538	2.56	−18.92
3460	1.46	−16.83
3483	2.24	−22.35
3752	2.17	−21.14
3799	1.46	−19.23
3844	2.60	−21.75
3881	0.01	−8.20
4616	1.47	−20.22
4860	3.55	−20.38
4999	1.36	−18.90
5107	3.52	−18.69
5190	1.35	−20.81
5501	0.01	−8.70
5620	0.21	−16.18
5685	0.55	−17.10
5748	1.97	−19.90
5827	1.66	−21.11
5837	2.28	−18.19
5878	2.50	−21.30
6056	0.67	−16.87
6396	2.64	−18.45
6438	2.60	−20.91
6821	1.12	−20.55
7905	0.71	−17.66

The model colors were obtained by integration over the low resolution spectra in Bruzual & Charlot (2003), weighted by the Gunn filter functions (i.e., SDSS filters). We assume a constant star formation rate back to some starting time, which is considered to be the region age. A range of extinctions was used for the models, following the wavelength dependencies in Calzetti et al. (2000) and Leitherer et al. (2002).

The average observed colors of all the Kiso clumps, averaged over the three apertures described below, were $\langle u-g\rangle = 0.67 \pm 0.63$, $\langle g-r\rangle = 0.22 \pm 0.30$, $\langle r-i\rangle = -0.08 \pm 0.37$, and $\langle i-z\rangle = -0.04 \pm 0.58$. For the SDSS clumps, the average colors were 0.39 ± 0.54, 0.18 ± 0.33, -0.20 ± 0.41, and 0.06 ± 0.43, respectively.

The final values for mass, age, and extinction were determined from weighted averages of trial models using a weighting function $e^{-0.5\epsilon\chi^2}$ for χ^2 equal to the quadratic sum of the differences between the model and observed colors, normalized to the dispersions for each color, and for $\epsilon = 0.01$. The factor ϵ makes the weighting function smooth considering the fact that there are many systematic uncertainties in addition to the statistical uncertainty of noise in the measured colors. The weighted averages were done only for the models with the lowest rms deviations from the observations, as determined by binning the rms deviations in intervals of 0.02. The average number of models that enter into each best-fit result is 160 ± 130. The sum of the squares of the differences between the four observed colors and the model colors has an rms of 0.05 ± 0.06.

Once the best-fit age and extinction are determined, the clump mass follows from the observed g magnitude in comparison to the model. The surface densities of star formation in the clumps are then calculated from the ratios of the masses to the projected areas that are used to measure the magnitudes. The telescope resolution determines a lower limit to the measurable size of a clump and the true sizes are smaller than the measured sizes. Using stars in several SDSS fields near our galaxies to determine instrumental resolution, we measured an average stellar Gaussian sigma value of about 1.2 pixels, depending slightly on passband. For an aperture size of 3 pixels, the intrinsic source size would be approximately 2.7 pixels if we subtract the resolution in quadrature. The intrinsic area would be smaller by 16%. Instrumental resolution does not affect the clump luminosity by a significant amount, so the primary effect of this correction is to increase the derived surface densities by an average factor of 1.16. In the plotted surface densities, we do not include this increase because it is a small effect compared to the other uncertainties, but in the determination of turbulent speed from the surface density, we make this correction, as discussed in Section 2.2.1.

For comparison with the Kiso clumps, clump properties in 30 clumpy galaxies (Table 3) in the Hubble UDF field, selected from Elmegreen et al. (2005b), were determined from Advanced Camera for Surveys (ACS) measurements in B_{435}, V_{606}, i_{775}, and z_{850} bands using the IRAF task *imstat*, which defines a rectangle around the clump and measures the total light inside the rectangle. The interclump background was measured from relatively clear regions nearby and subtracted from the clump light. The same clump and interclump rectangle was used for all passbands. The task *apphot* is not good for highly clumpy galaxies because the background annulus may contain parts of other clumps. Still, a comparison of the color measurements using *imstat* and *apphot* for two UDF galaxies showed an average difference of only 0.01, 0.03, and 0.07 mag for $B-V$, $V-i$, and $i-z$, respectively.

The 30 UDF galaxies were chosen from our catalog (Elmegreen et al. 2005b) of 178 "clump clusters"—so named

before their kinematics (Förster-Schreiber et al. 2006; Weiner et al. 2006; Genzel et al. 2006) showed them to be whole galaxies of an extremely clumpy type not commonly observed in the local universe. We avoided the more amorphous types and picked those with distinct clumps, fairly large in angle, not obviously interacting, and not highly inclined. They span the same range of restframe absolute *B*-band magnitude as the Kiso clumpy and local spiral galaxies.

The clump properties for UDF galaxies were determined following the same procedure as for the Kiso galaxies but with redshift corrections and corrections for intervening H I (Madau 1995). The redshifts were photometric and taken from Rafelski et al. (2009). Because high-redshift galaxies have slightly lower metallicities for the same luminosity as local galaxies (e.g., Mannucci et al. 2009), we assumed a metallicity of 0.4 solar in the Bruzual & Charlot (2003) tabulations.

As for the Kiso galaxies, telescope resolution limitations imply that the intrinsic source size is smaller than the measured size. We measured an average Gaussian sigma for stars in the ACS UDF field to be 3.14 pixels. The average *imstat* area for the UDF clumps is 34.5 square pixels, and the average deconvolved area is 24.6 square pixels. Thus the intrinsic clump areas are on average 1.4 times smaller than the measured areas. This increases the derived surface densities by the same factor. This factor is included in the determination of turbulent speeds below.

To compare star formation with global properties, we determined absolute restframe *B*-band integrated galaxy magnitudes by interpolating the ACS filters. Restframe *B*-band magnitudes were determined for the Kiso and local spiral galaxy samples by interpolation and conversion in the SDSS filters.

We do not discuss individual clump ages below, but note that for Kiso clumps, the average log-age (in years) is 7.1 ± 1.3 for each aperture size, and for the SDSS galaxy clumps, it is 6.8 ± 1.2 for each aperture size. For all of the non-bulge UDF clumps, the average log-age is 7.8 ± 0.8. Therefore, all of the clumps have similar ages within the dispersions. They are significantly younger than a Gyr and typically range between 10 Myr for local galaxies and 100 Myr for UDF galaxies.

We also do not discuss individual extinctions below. The average fitted extinction for all of the measured clumps in the Kiso galaxies is 1.6 ± 0.5 mag in the *V* band; for the SDSS galaxies it is 1.5 ± 0.6 mag, and for the UDF galaxies it is 2.3 ± 2.0 mag. The extinctions for UDF galaxies are fairly inaccurate without observer-frame red measurements, but we cannot use the *Hubble Space Telescope* (*HST*) in the *JHK* bands because the angular resolution is too low to resolve any but the most massive clumps (it is three times worse than the ACS resolution in optical bands). The masses and surface densities discussed below have been corrected for the extinction determined by each fit.

The derived extinctions may appear to be small for massive star-forming regions, but the pressures from young stars should drive gas and dust away from the line of sight, as it does in local starbursts (Maiz-Apellaniz et al. 1998). Our extinctions are comparable to those of super star clusters in the center of M82, which is the prototype of a highly extincted nearby starburst galaxy. The internal extinction for 200 super star clusters in the center of M82 ranges from 1.5 to 6 mag in the *V* band (Melo et al. 2005). The average extinction over big sections of typical galaxies is smaller than this. We computed the effective mean extinction in the central regions of the Kiso galaxies from the Balmer decrements in the SDSS fiber spectra (3″ diameter) using the formula $A_V = 8 \log(H\alpha/(2.86 H\beta)$ (Dominguez et al. 2013). The average for all of the Kiso galaxies in our survey is $A_V = 0.55 \pm 0.45$ mag. The largest extinction of $A_V = 1.7$ mag corresponds to Kiso 8708. Large-scale effective mean extinctions in spiral galaxies depend on mass but are also on the order of $A_V = 1$ mag (e.g., Garn & Best 2010). These large-scale effective mean extinctions are smaller than the extinctions to star forming regions because the large scale dust distribution varies across a large region and the proportion of light coming from lower-than-average extinctions outweighs the proportion coming from higher-than-average extinctions (Fischera et al. 2003).

2.2. Clump Results

2.2.1. Mass, Surface Density, and the Jeans Relations

Figure 4 shows in the bottom three panels the non-bulge clump masses plotted versus the absolute *B*-band magnitudes of the whole galaxies in all three samples. In the top panels, the projected surface densities are shown. The lines in each panel show the linear fits to the data (on these log–log plots). The fit to the UDF galaxies, shown as a dotted line in the left panels, is reproduced in the center panel for comparison with the Kiso galaxies. Similarly, the fit to the local galaxies, a dashed line in the right-hand panels, is again in the center panels. The solid line is the fit to the Kiso galaxies. These fits are for clump mass $m_{\rm clump}$ and surface density $\Sigma_{\rm clump}$,

$$\log m_{\rm clump} = 3.64 - 0.18 M_B \text{ (UDF)}; -3.57 - 0.54 M_B \text{ (Kiso)}; \\ -3.05 - 0.41 M_B \text{ (Normal)} \quad (1)$$

$$\log \Sigma_{\rm clump} = -1.19 - 0.12 M_B \text{ (UDF)}; -2.41 - 0.18 M_B \text{(Kiso)}; \\ -0.61 - 0.063 M_B \text{ (Normal)}. \quad (2)$$

The UDF galaxies reach brighter absolute restframe *B* magnitudes than the Kiso galaxies, and the most massive UDF clumps are more massive than the most massive Kiso galaxy clumps. Also at low luminosity, the UDF clumps are more massive than most of the Kiso clumps in galaxies of the same luminosity. However, the most luminous Kiso galaxies have clumps that are comparable in mass and column density to clumps in UDF galaxies at the same luminosity. In this respect, the most luminous Kiso galaxies are comparable to UDF clumpy galaxies of the same luminosity. Note that both types have clumps measured in the same way and use the same population synthesis and extinction models.

Normal local galaxies, on the other hand, have clumps that are much lower in mass than the clumps in either the UDF or Kiso galaxies. This is to be expected because the UDF and Kiso galaxies were chosen to be clumpy types, while the local galaxies were not. At a given luminosity, the clumps in the Kiso galaxies are typically 30 to 100 times more massive than the star forming regions in local galaxies.

Uncertainties in the various assumptions that have been made for the population synthesis models of clump properties should not significantly affect the results in Figure 4. We assumed solar metallicity for the local and Kiso galaxies, and 0.4 times the solar metallicity for the UDF galaxies. These are reasonable assumptions considering the higher star formation rates at the same stellar mass in UDF galaxies (e.g., Mannucci et al. 2010), but if the average metallicity of the UDF galaxies were different, then the derived masses could be different too. The effect is

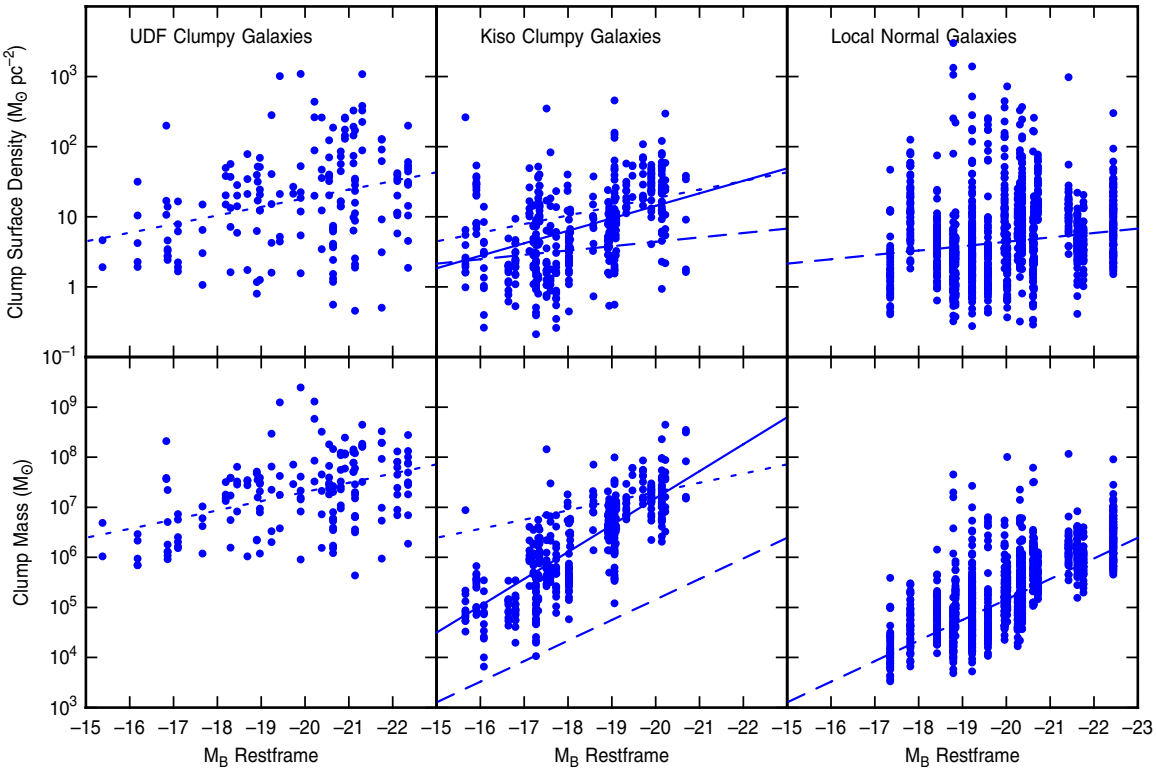

Figure 4. Mass (bottom) and surface density (top) of clumps in UDF (left), Kiso (middle), and normal spiral galaxies (right), plotted versus the absolute restframe *B* magnitude of the whole galaxy. Fits to the data are shown in each panel, with the fits in the central panels shown by solid lines and the fits to the UDF and normal clumps repeated in the central panels for comparison.

(A color version of this figure is available in the online journal.)

small, however. Elmegreen et al. (2009a) showed that a decrease in metallicity from 0.008 to 0.0004 increases the mass and age by only 50% each as a result of a decrease in line-blanketing and bluer intrinsic colors. Uncertainties in extinction affect the age more than the mass. Higher extinction requires bluer and younger stellar regions to give the same color, but these younger regions have higher light-to-mass ratios which offset the greater extinction, giving about the same required mass (Bell & de Jong 2001). As a result, the mass uncertainties from both extinction and metallicity uncertainties are much less than the differences in mass between the three groups of galaxies in Figure 4.

2.2.2. The Jeans Mass and Implications for Gas Velocity Dispersion

If the star-forming clumps in all of these galaxies can be identified with the ambient Jeans mass in the disks, and if this mass varies as σ^4/Σ for gas velocity dispersion σ and mass column density Σ, then we can use the results in Figure 4 to see how σ and Σ vary from normal galaxies to Kiso clumpy galaxies to UDF clumpy galaxies. First, consider the low luminosity galaxies, $M_B = -16$, where the UDF clumps are more massive than the Kiso clumps by a factor of $\sim$28 according to Equation (1), and the UDF clump column densities are higher than the Kiso clump column densities by a factor of $\sim$1.8 according to Equation (2). Resolution effects discussed above suggest that the intrinsic UDF clump column densities are higher than the observed by an average factor of 1.4, and the KISO column densities are higher than the intrinsic by a factor of 1.16. Thus the intrinsic column density ratio should be corrected upward by a factor of $1.4/1.16 = 1.2$. We therefore take $\Sigma_{\rm UDF}/\Sigma_{\rm Kiso} = 2.2$. Scaling these observed stellar column densities to the Jean gas column densities (which assumes a fixed star formation efficiency), we get a ratio of velocity dispersions from this and from the ratio of the UDF clump mass, $m_{\rm UDF}$, to the Kiso clump mass, $m_{\rm Kiso}$,

$$\frac{\sigma_{\rm UDF}}{\sigma_{\rm Kiso}} = \left(\frac{\Sigma_{\rm UDF}}{\Sigma_{\rm Kiso}} \times \frac{m_{\rm UDF}}{m_{\rm Kiso}}\right)^{0.25} \sim 2.8. \quad (3)$$

Comparing the Kiso clumps to normal galaxy clumps in the same way for $M_{\rm B} = -16$, we see that $m_{\rm Kiso}/m_{\rm normal} \sim 36$ and $\Sigma_{\rm Kiso}/\Sigma_{\rm normal} \sim 1.4$ for the resolution-corrected $\Sigma_{\rm Kiso}$, in which case $\sigma_{\rm Kiso}/\sigma_{\rm normal} \sim 2.7$. Thus at low luminosity, the mass column density of star forming material and the resulting star complexes increase by factors of 1.4 and 2.2 going from normal galaxies to Kiso clumpy galaxies to UDF clumpy galaxies, and the gaseous velocity dispersion increases by factors of 2.7 and 2.8 again along this same sequence.

At high luminosity, $M_{\rm B} = -20$, the UDF and Kiso clump masses and column densities are about the same, $m_{\rm UDF}/m_{\rm Kiso} = 1.0$, and $\Sigma_{\rm UDF}/\Sigma_{\rm Kiso} = 1.3$ (corrected), so the velocity dispersions also have to be about the same in the Jeans model, $\sigma_{\rm UDF}/\sigma_{\rm Kiso} = 1.1$. There is a big jump in clump properties from normal to Kiso clumpy galaxies, however. Figure 4 and Equation (1) suggests that $m_{\rm Kiso}/m_{\rm normal} \sim 120$ at $M_{\rm B} = -20$ and $\Sigma_{\rm Kiso}/\Sigma_{\rm normal} \sim 4.0$ (corrected Kiso), which means that $\sigma_{\rm Kiso}/\sigma_{\rm normal} \sim 4.7$. Thus at high luminosity, Σ increases by factors of 4.0 and 1.3 going from normal to Kiso clumpy to UDF clumpy, while σ increases by factors of 4.7 and 1.1 in this sequence.

According to this scenario, the velocity dispersion in Kiso galaxies is higher than in normal galaxies by factors ranging from 2.7 to 4.7, with the most luminous Kiso galaxies having the highest excess dispersions. The column densities in Kiso

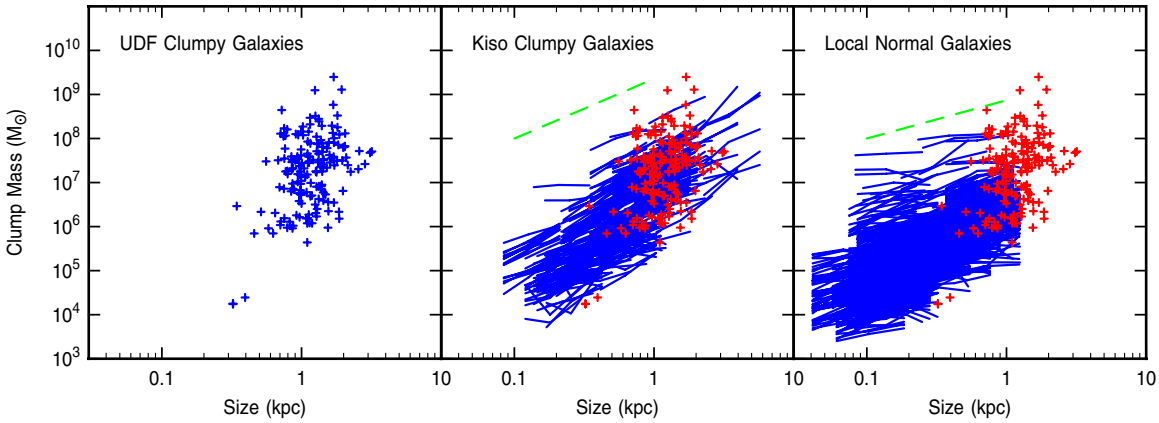

Figure 5. Clump masses are shown as functions of the clump sizes (diameters) for the three galaxy types. For Kiso and normal galaxies, the clumps were measured at three different radii: 2, 3, and 5 pixels for Kiso galaxies, and 3, 5, and 9 pixels for normal spiral galaxies. The lines in each figure connect these three measurements for each clump; the green dashed lines show the average slopes of mass versus size (1.36 for Kiso galaxies and 0.87 for local galaxies). The UDF mass–size distribution is shown in the center and right panels as a collection of red plus signs for comparison.

(A color version of this figure is available in the online journal.)

galaxies are higher than in normal galaxies by factors ranging from 1.4 to 4.0, with the higher excess again in the most luminous Kiso galaxies. The column densities and velocity dispersions are higher still in UDF galaxies compared to normal galaxies, as already known (see review in Shapley 2011). Thus the clumpy Kiso galaxies are intermediate between normal galaxies and UDF clumpy galaxies at low luminosity, and they are similar in clump properties to UDF galaxies at high luminosity.

2.2.3. Mass and Size

Figure 5 shows the clump masses as functions of their physical sizes for all three galaxy types. The UDF clumps are shown on the left and repeated as red plus signs in the middle and right hand panels for comparison to the Kiso and normal galaxy clumps. As noted in the figure caption, the Kiso and normal galaxy clumps were measured with three different angular radii, so the masses are shown for each size as connected lines. The sizes, given in kiloparsecs, are proportional to the galaxy distances. The average slope of all the lines is shown as a dashed green line in the middle and right hand panels. These slopes are 1.36 and 0.87 for Kiso and normal galaxies, respectively.

The trend of increasing mass with clump size is not the result of background emission because the average background has been removed by the IRAF routine *apphot*. It is the result of tapered light profiles in the clumps. The average surface density decreases by a factor of ∼2 from the minimum to the maximum clump size in each survey, considering the scaling of mass with size.

The UDF clumps are all fairly large, >0.5 kpc, partly as a result of limited spatial resolution at intermediate redshifts. Similarly large clumps are in the Kiso galaxies, although their masses are slightly lower for a given size (consistent with the lower Σ for Kiso clumps, as discussed above). In addition, the largest Kiso clumps have the same mass as the largest UDF clumps, although the sizes of these largest Kiso clumps are larger than the sizes of the largest UDF clumps (the Σ difference again).

Star-forming complexes in normal galaxies tend to be smaller than the largest clumps in either UDF clumpy galaxies or Kiso clumpy galaxies, but where they overlap in size, the clumps in normal galaxies are less massive than clumps of the same size in UDF galaxies (again this is the Σ difference discussed above).

Clump size in the Jeans model scales with σ^2/Σ. If at high luminosity, Σ is in the sequence 1:4.0:5.1 for normal:Kiso:UDF galaxies and σ is in the sequence 1:4.7:5.0, as derived above, then size is in the sequence 1:5.5:4.9, which is about what Figure 5 shows, i.e., both Kiso and UDF galaxies have physically larger clumps than normal galaxies, by a factor of 3–10. At low luminosity, for the above sequences of Σ (1:1.4:3.0) and σ (1:2.7:7.4), the Jeans size increases in the sequence 1:5.2:18.4 from normal to Kiso to UDF galaxies.

3. STAR FORMATION RATES

The average star formation rates were determined for each clump in all three samples by taking the ratio of clump mass to age. In addition, the current star formation rates for Kiso galaxies were determined from the Hα equivalent widths in the SDSS fiber spectra. These spectra have a resolution of ∼150 km s^{-1} at Hα and an angular size of 3″ (0.16 to 3 kpc for our distances), centered on the galaxy. The Hα fluxes for the full galaxies were estimated from the Hα equivalent widths in the fiber multiplied by the *r*-band luminosities of the galaxies. This procedure assumes that the full galaxy is forming stars at the rate of the central 3″. The corresponding star formation rates were inferred from the total Hα fluxes using the conversion in Kennicutt (1998).

Figure 6 shows the star formation rates for the three types of galaxies studied here. The rates determined from the ratios of mass to age are the dots. The rates determined for the Kiso galaxies from the Hα equivalent widths in the central 3″ extrapolated to the whole galaxy are the red squares in the center panel. The lines show the linear fits (for these log–log plots), with the fits for UDF and normal galaxies repeated in the central panel for comparison, as in Figure 4. The similarity for Kiso galaxies between the star formation rates in individual clumps and the extrapolated whole galaxy rates suggest that the measurements in the central 3″ fibers are not representative of the most active clumpy regions, which are often at the outskirts.

The star formation rates in UDF and Kiso clumps are about the same for a given restframe absolute *B* magnitude. The rates are systematically lower in the normal galaxies by a factor of 10–30. This lower rate for normal galaxy clumps reflects the lower masses of the clumps.

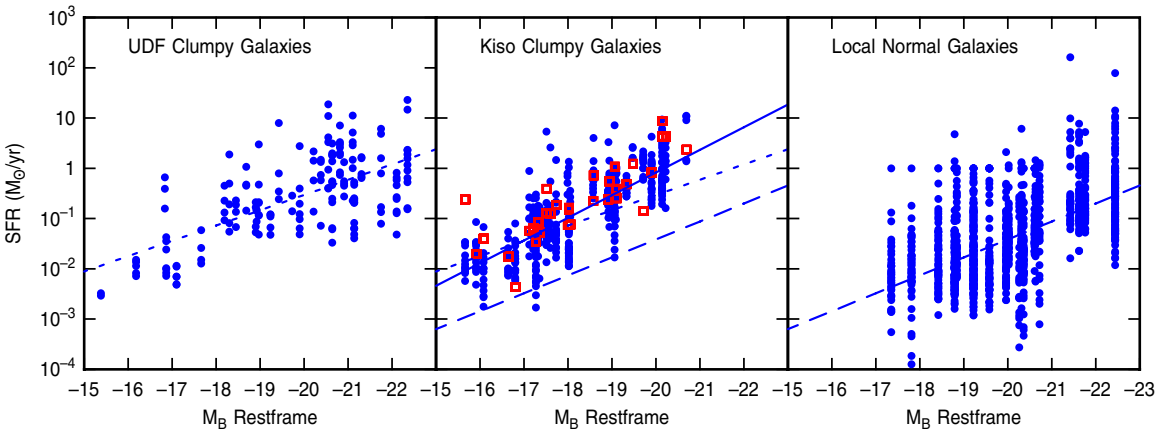

Figure 6. Clump star formation rates in $M_\odot$ yr^{-1} are shown versus the absolute restframe B magnitudes of the whole galaxies for all three galaxy types. The fits to the points are indicted, with the UDF and normal galaxy fits repeated in the central panel for comparison. The red squares in the central panel are star formation rates for the whole Kiso galaxies determined from the product of the Hα equivalent width in the SDSS fiber and the SDSS r-band luminosity of the galaxy.
(A color version of this figure is available in the online journal.)

4. COMPARISON WITH OTHER STUDIES

The trends in Figure 4 and in the above discussion are consistent with those in Wisnioski et al. (2012) in the sense that larger clumps in both radius and mass also have higher velocity dispersions, with a smooth trend going from local star-forming regions to those at $z \sim 1$–2. Wisnioski et al. (2012) measured velocity dispersions from Hα emission in H II regions, while our dispersions are assumed to represent neutral gas before gravitational instabilities make clumps. The high-redshift clumps in Wisnioski et al. (2012) have sizes that are larger than ours by a factor of ∼2, and dispersions of 50–150 km s^{-1}, increasing with size to the power 0.42. Our UDF clumps have dispersions ∼5 times larger than clumps in local galaxies, which converts to ∼50–75 km s^{-1}. Thus the upper range for our dispersions is comparable to the lower range for the Wisnioski et al. (2012) dispersions. This difference is not unreasonable considering our lower clump sizes and the different phases of interstellar gas used for the probes.

Also for Wisnioski et al. (2012), the galaxies with clump sizes and masses between those of normal local galaxies and high redshift clumpy galaxies were major mergers (from Monreal Ibero et al. 2007). In the present paper, they are Kiso types Ic and Ig, chosen to be unlike mergers by their lack of obvious tidal features or peripheral asymmetries. Still, the Kiso galaxies apparently have high gas velocity dispersions, perhaps related to the generally asymmetric positions of their inner red bulges and disks (Figures 1–3).

The clumps in five $z \sim 2$ galaxies studied by Genzel et al. (2011) are more massive than those here because they choose regions that are bright enough to give spectra. Their galaxies are generally brighter and more massive too: the galactic restframe V-band AB magnitudes in their study averaged ~ -23 (Förster Schreiber et al. 2009) compared to our brightest B-band AB magnitude of ∼−20 in the region of overlap with the Kiso sample.

5. RADIAL PROFILES

The Kiso galaxies in our sample have approximately exponential light profiles. Figure 7 shows ellipse-fit average radial profiles for the Kiso galaxies. The number of scale lengths in the Kiso exponentials are given in the figure next to each Kiso name. Some of the Kiso galaxies have a change of slope partway out in their disks, indicating a double exponential. In most cases, these galaxies have off-center bulges, so the exponential profile is normal until the radius of the limit of symmetry is reached, and then the slope changes beyond (see, e.g., Kiso 7186).

The major axis intensity profiles of Kiso galaxies are slightly more irregular than the azimuthally averaged radial profiles because of the clumps, but the underlying disks in Kiso galaxies are still exponential. Figure 8 shows these major axis profiles. Some galaxies have clumps in the g-band that are as prominent as the bulges (e.g., Kiso 4291, 4876, 5506, 5886, 5979, 6630, 8116).

Figures 9 and 10 show the average radial profiles from ellipse fits and major axis profiles, respectively, for the UDF galaxies studied here. The strips used for the major axis scans are indicated on images of the galaxies in Figures 11 and 12. The profiles were corrected for surface brightness dimming by multiplying each intensity by $(1 + z)^4$ for corresponding redshift z. They were not put in a common restframe wavelength, however, because unlike the total galaxy magnitudes, the high-resolution images of UDF galaxies have only optical coverage in the ACS bands. Thus there is an unavoidable shift toward shorter wavelength restframes with increasing redshift.

The average radial profiles of the UDF galaxies are roughly exponential (the number of scale lengths is given in parenthesis), although the major axis strips are usually irregular because of the clumps (and especially so because the restframe wavelengths tend to be blue or UV). Many UDF galaxies are ring-like (Elmegreen et al. 2009a) and their centers are hard to define for the average profiles, but if the galaxies have bulge-like clumps near their centers then the average light profiles away from these clumps are somewhat exponential. The average radial positions of the clump centers are also exponential on average for the clumpy UDF galaxies, as found in an earlier study (Elmegreen et al. 2005a).

Figures 13–15 show three normal spirals, a grand design (NGC 5248), multiple arm (NGC 3344), and a flocculent (NGC 5055), for comparison. Figure 13 has SDSS sky images with the same color scheme as in Figures 1–3, Figure 14 shows the ellipse fit radial profiles on the left and major axis scans on the right, and Figure 15 shows the scan directions for the major axis profiles. The normal galaxies differ from the Kiso and UDF galaxies because the normals have a more prominent bulge and a smoother radial profile than the other types (the sharp peaks

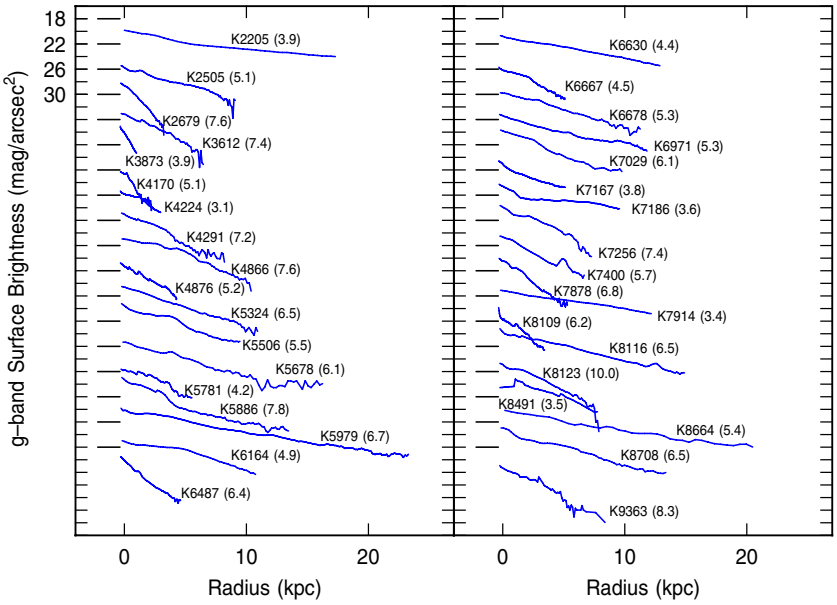

Figure 7. Radial profiles of azimuthally averaged light in *g*-band are shown for all Kiso galaxies studied here. The profiles are approximately exponential but there are sometimes large local excesses at the radii of the clumps. The Kiso numbers are indicated with the number of exponential scale lengths in the whole profile given in parentheses. The vertical axis tickmarks are separated by 2 mag arcsec^{-2} of surface brightness. Each scan has a different vertical shift in this plot. The tickmarks on the left in each panel indicate a surface brightness of 18 mag arcsec^{-2} for the corresponding scan, which usually comes close to touching it. The numerical labels at the top left correspond to the surface brightness scale of the top profile, i.e., for Kiso 2205.

(A color version of this figure is available in the online journal.)

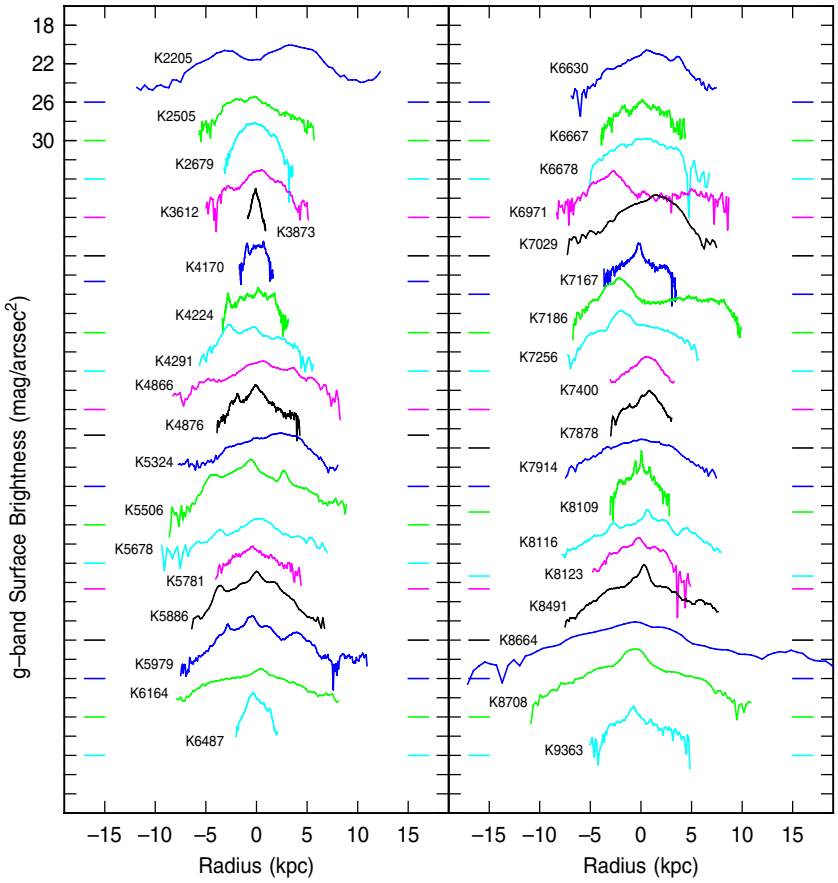

Figure 8. Major axis scans through the Kiso galaxies in the *g* band are shown versus position in kpc, with zero position at the center of the scan. The clumps are more prominent in these single-direction scans than in the average radial profiles in the previous figure. Still, most Kiso galaxies have a smooth component to the disk with an approximately exponential profile. The vertical axis tickmarks are separated by 2 mag arcsec^{-2} of surface brightness. Each scan has a different vertical shift. The colored tickmarks on the left and right of each panel indicate a surface brightness of 26 mag arcsec^{-2} for the corresponding scan, which has the same color. Sometimes the scans are shifted up and down slightly so they do not overlap. The numerical labels at the top left correspond to the surface brightness scale of the top profile, i.e., for Kiso 2205.

(A color version of this figure is available in the online journal.)

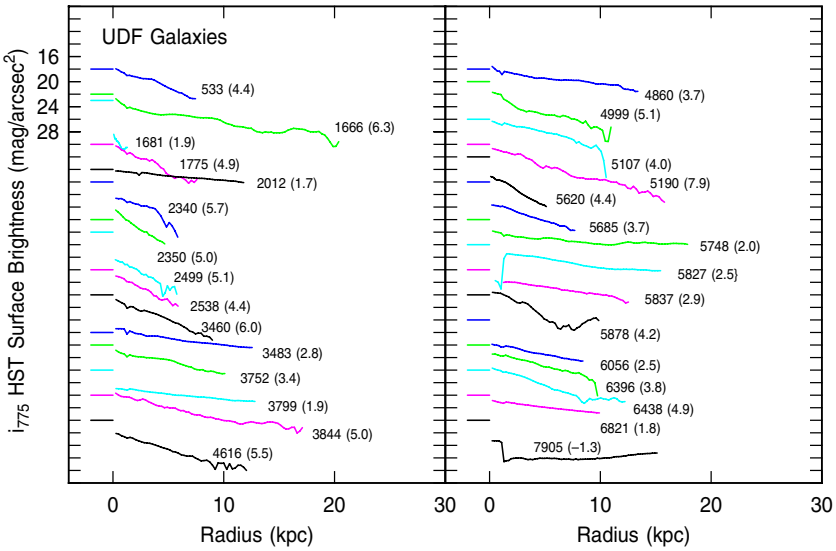

Figure 9. Radial profiles of azimuthally averaged light in the *HST* i_{775}-band are shown for all UDF galaxies studied here. The profiles are sometimes exponential but there are usually large local excesses at the radii of the clumps. The UDF numbers are indicated with the number of exponential scale lengths in the whole profile given in parentheses. The vertical axis tickmarks are separated by 2 mag arcsec^{-2} of surface brightness. Each scan has a different vertical shift. The tickmarks on the left in each panel indicate a surface brightness of 18 mag arcsec^{-2} for the corresponding scan, which has the same color and usually comes close to touching it. Sometimes the scans are shifted up and down slightly so they do not overlap. The numerical labels at the top left correspond to the surface brightness scale of the top profile, i.e., for UDF 533. For the determination of the number of scale lengths indicated in parentheses, we ignored the rapidly changing inner parts in galaxies 5827 and 7905, and the rapidly changing outer parts in 5107 and 6396. The scans have been corrected for surface brightness dimming but not interpolated to a common restframe wavelength.

(A color version of this figure is available in the online journal.)

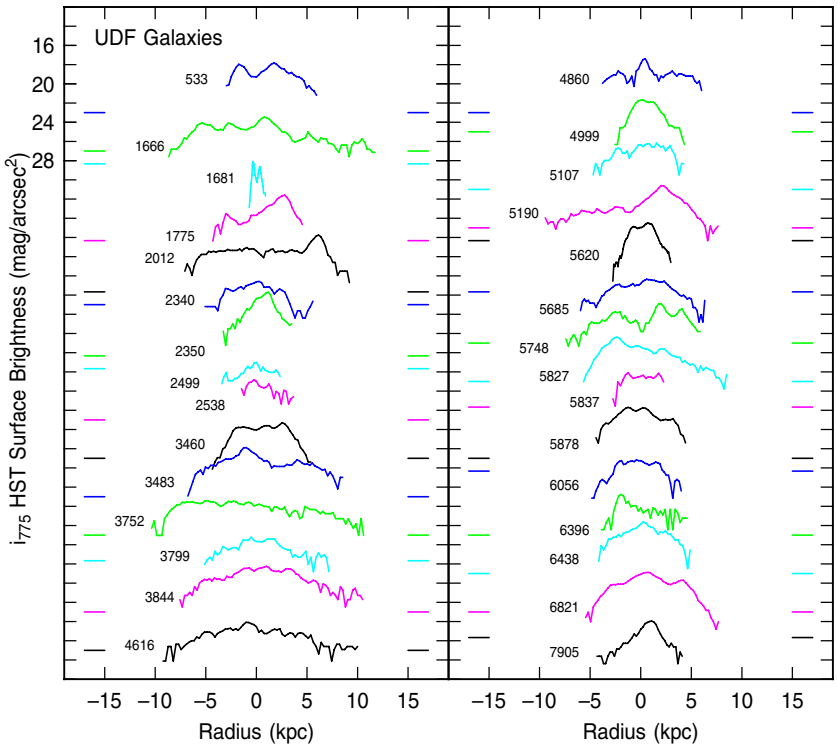

Figure 10. Linear scans through the UDF galaxies (with scan directions shown in the two following figures) in the *HST* i_{775}-band are shown versus position in kiloparsecs with zero position at the center of the scan. The clumps are more prominent in these single-direction scans than in the average radial profiles in the previous figure. Many UDF galaxies have no semblance of a smooth underlying component and no exponential profile. The vertical axis tickmarks are separated by 2 mag arcsec^{-2} of surface brightness. Each scan has a different vertical shift. The colored tickmarks on the left and right of each panel indicate a surface brightness of 23 mag arcsec^{-2} for the corresponding scan, which has the same color. Sometimes the scans are shifted up and down slightly from a more regular positioning so that they do not overlap. The numerical labels at the top left correspond to the surface brightness scale of the top profile, i.e., for UDF 533. The scans have been corrected for surface brightness dimming but not interpolated to a common restframe wavelength.

(A color version of this figure is available in the online journal.)

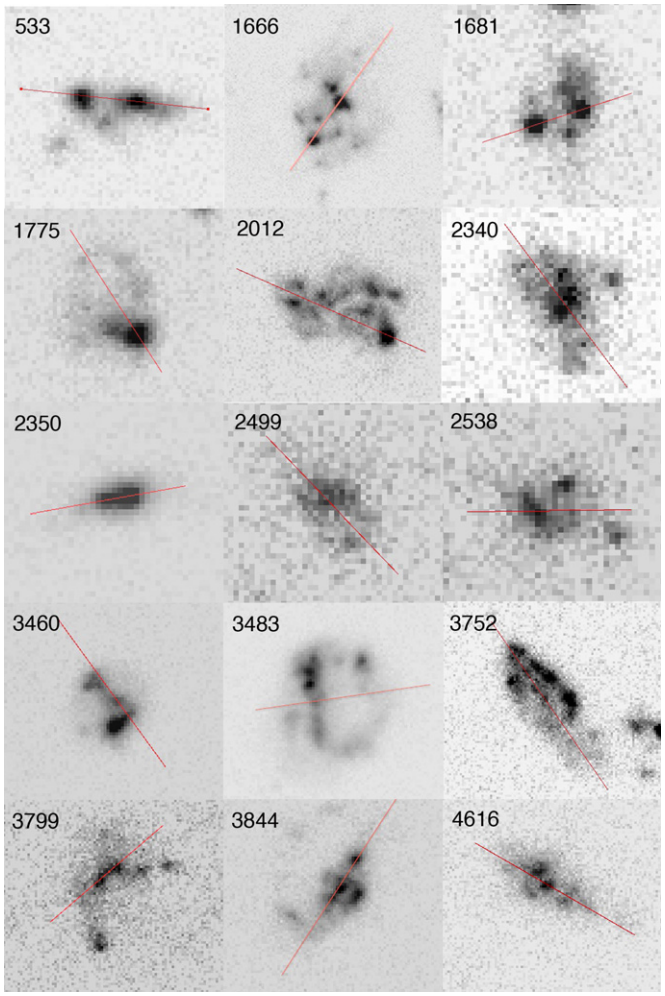

Figure 11. Images of the UDF clumpy galaxies studied here with lines showing the positions of the linear scans used for Figure 10. The passband is i_{775}.
(A color version of this figure is available in the online journal.)

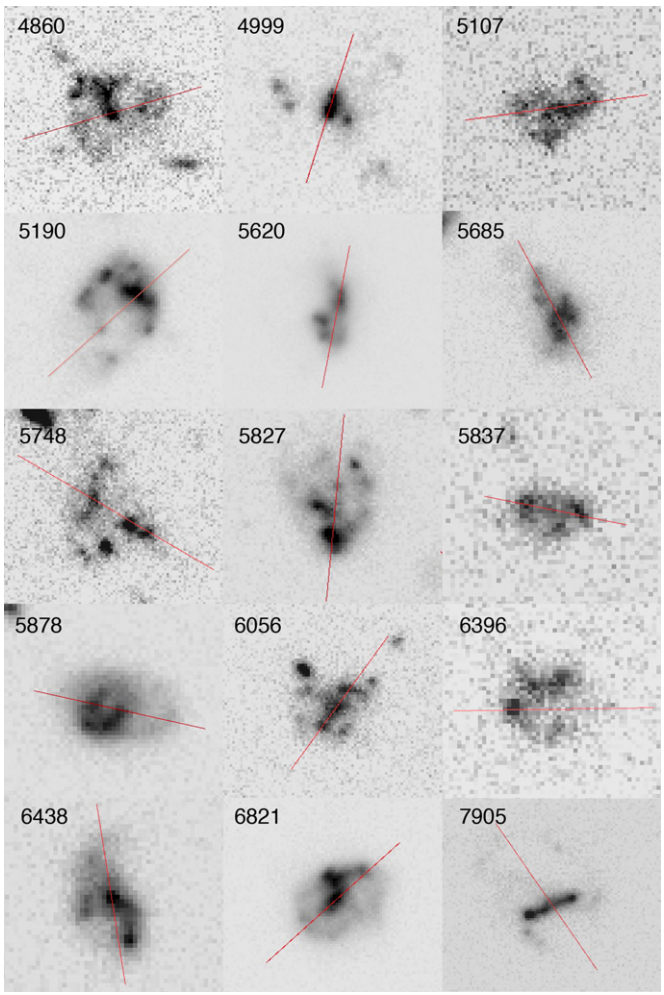

Figure 12. Images of the UDF clumpy galaxies studied here with lines showing the positions of the linear scans used for Figure 10. The passband is i_{775}.
(A color version of this figure is available in the online journal.)

in the ellipse fits for NGC 3344 and NGC 5248 are foreground stars). This smoothness is consistent with the previous result that the non-bulge clumps in normal galaxies are smaller than those in Kiso and UDF galaxies.

6. DISCUSSION

We find that the brightest Kiso galaxies have giant non-bulge clumps that are similar in mass and surface density to the non-bulge clumps in high-redshift clumpy galaxies of the same absolute restframe *B* magnitude. The local normal galaxies have much smaller clumps than either of these. This trend in clump mass and surface density is consistent with a steady decrease over time in average gas surface density and turbulent speed in disk galaxies, leading to a corresponding decrease in the Jeans mass.

The high mass clumps in the Kiso galaxies are often in spiral arms, but analogous arms cannot be seen in the clumpy UDF galaxies. Part of the difference in UDF structure could be from the lack of sufficiently deep, high resolution restframe *V*-band or redder observations, where local galaxies show spiral structure in the old disk stars. However, the restframe UV sampled in the clumpy UDF galaxies does not show spiral features either, whereas *Galaxy Evolution Explorer* UV images of local galaxies do show spiral arms, even if only in the alignment of clumps. In addition, clumpy galaxies without spirals were found in lower-redshift surveys too (Elmegreen et al. 2009b), in a redshift range overlapping that of local spiral galaxies, and in those clumpy galaxies their restframe *B*- or *V*-band images have sufficiently high resolution and depth in the ACS camera to have shown spirals if they were present.

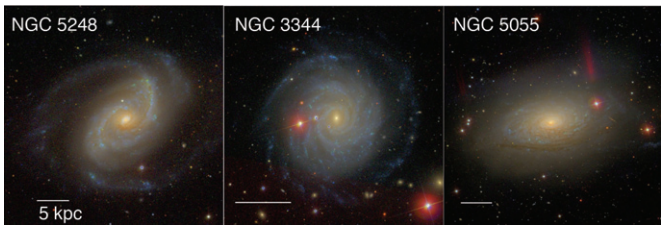

Figure 13. SDSS images in *g*, *r*, and *i* passbands of three local galaxies that were used to compare the radial profiles with those of clumpy Kiso and UDF galaxies.
(A color version of this figure is available in the online journal.)

Kiso galaxies are also midway between UDF and normal galaxies with respect to the average radial disk profiles. While all three types have roughly exponential profiles for azimuthally-averaged light when measured with increasing distance from the brightest clumps or bulge-like centers, UDF galaxies viewed in restframe blue or UV light have the most irregularity in

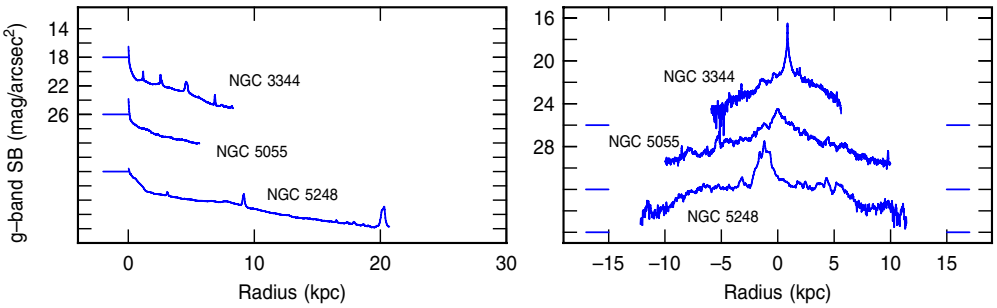

Figure 14. Ellipse-fit radial profiles (left) and major axis scans (right) for three local spiral galaxies, in the *g* band. Each profile is shifted vertically in this plot for clarity, with the *y*-axis numbers corresponding to the top profile. The horizontal marks at negative radii are at surface brightnesses of 18 mag arcsec^{-1} on the left, and 26 mag arcsec^{-1} on the right. The major axis profiles are centered on the midpoints of the scans, not the galaxy centers.

(A color version of this figure is available in the online journal.)

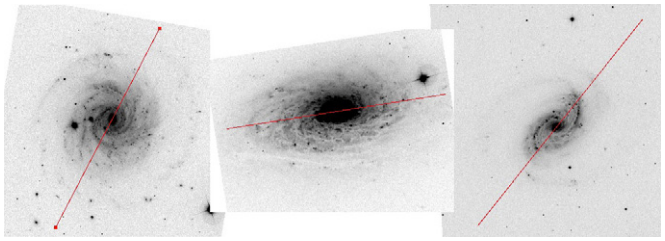

Figure 15. Scan directions for the local spiral intensity profiles shown in the previous figure. The images are in the *g* band from the SDSS.

(A color version of this figure is available in the online journal.)

these profiles, with Kiso galaxies next. Even more extreme are major axis intensity scans, which are highly irregular in the UDF clumpy galaxies and still irregular but less so in the Kiso galaxies.

Galaxy evolution is characterized by the simultaneous build up of an old stellar disk and the loss of giant star-forming clumps. Such clumps are still possible in the local universe in exceptional circumstances, presumably when the gas becomes highly turbulent. The giant clumps in the Kiso galaxies, for example, are mostly in spiral arms, where even local galaxies have somewhat massive clumps, whereas high redshift clumpy galaxies do not have spirals. The source of the presumed high turbulence in clumpy Kiso galaxies could be related the overall disk asymmetry.

7. CONCLUSIONS

Star forming complexes and radial disk profiles were studied in three samples of clumpy irregular galaxies, one at high redshift using the Hubble UDF, and two at low redshift using UV-bright Kiso galaxies and normal spirals. The brightest Kiso galaxies have clump masses and surface densities comparable to those at high redshift for the same absolute restframe *B*-band magnitude. These two types also have irregular radial profiles because of the clumps, although the UDF galaxies are more irregular. Normal local spirals have smoother profiles and clumps that are lower in mass by a factor of ∼100. Clump ages in the Kiso and local spiral galaxies are on the order of 10 Myr, with slightly older ages for the UDF clumps.

If the clumps have masses comparable to the local Jeans mass, then this mass is related to the clump surface density and velocity dispersion. Using this relation, we determine that the interstellar velocity dispersion increases from local spirals to Kiso clumpies to UDF clumpies in the proportion 1 to 4.7 to 5.0 for the most luminous galaxies in our sample, and in the proportion 1 to 2.7 to 7.4 for the least luminous, again for a given restframe absolute magnitude. The surface densities also increase along this sequence from 1 to 4.0 to 5.1 for the most luminous, and 1 to 1.4 to 3.0 for the least. We therefore predict that many of the clumpy Kiso types Ic and Ig will have elevated velocity dispersions and gas surface densities compared to local spiral galaxies. Considering both their clump properties and the radial profiles, Kiso galaxies are intermediate between highly clumpy UDF galaxies and local spirals.

Kiso galaxies are massive disk galaxies like local spirals, based on their absolute magnitudes, but they contain bigger and denser clumps than the spirals, and this makes them resemble young galaxies in the UDF. There is no reason to think that clumpy Kiso galaxies are young, so this morphological property can evidently be triggered in the modern universe by increasing the surface density and velocity dispersion in a galaxy. Such increases might result from a near encounter with another galaxy of comparable mass, or from other types of torquing, which stir the disk and lead to accretion. We note that most of the Kiso galaxies in our survey have bulges that are slightly offset from the center, and this asymmetry may drive turbulence and disk inflow also.

REFERENCES

Abazajian, K. N., Adelman-McCarthy, J. K., Agüeros, M. A., et al. 2009, ApJS, 182, 543
Abraham, R., van den Bergh, S., Glazebrook, K., et al. 1996, ApJS, 107, 1
Barden, M., Jahnke, K., & Häussler, B. 2008, ApJS, 175, 105
Bell, E. F., & de Jong, R. S. 2001, ApJ, 550, 212
Benvenuti, P., Casini, C., & Heidmann, J. 1982, MNRAS, 198, 825
Bothwell, M. S., Smail, I., Chapman, S. C., et al. 2013, MNRAS, 429, 3047
Bournaud, F., Elmegreen, B. G., & Elmegreen, D. M. 2007, ApJ, 670, 237
Brinks, E., & Klein, U. 1988, MNRAS, 231, P63
Bruzual, G., & Charlot, S. 2003, MNRAS, 344, 1000
Cacciato, M., Dekel, A., & Genel, S. 2012, MNRAS, 421, 818
Calzetti, D., Armus, L., Bohlin, R., et al. 2000, ApJ, 533, 682
Casini, C., & Heidmann, J. 1976, A&A, 47, 371
Casini, C., Heidmann, J., & Tarenghi, M. 1979, A&A, 73, 216
Ceverino, D., Dekel, A., & Bournaud, F. 2010, MNRAS, 404, 2151
Conselice, C. J., Blackburne, J. A., & Papovich, C. 2005, ApJ, 620, 564
Cresci, G., Mannucci, F., Maiolino, R., et al. 2010, Natur, 467, 811
Dominguez, A., Siana, B., Henry, A. L., et al. 2013, ApJ, 763, 145
Elmegreen, B. G., & Elmegreen, D. M. 2005, ApJ, 627, 632
Elmegreen, B. G., Elmegreen, D. M., Fernandez, M. X., & Lemonias, J. J. 2009a, ApJ, 692, 12
Elmegreen, B. G., Elmegreen, D. M., Vollbach, D. R., Foster, E. R., & Ferguson, T. E. 2005a, ApJ, 634, 101
Elmegreen, D. M., & Elmegreen, B. G. 1987, ApJ, 314, 3
Elmegreen, D. M., Elmegreen, B. G., & Hirst, A. C. 2004, ApJL, 604, L21
Elmegreen, D. M., Elmegreen, B. G., Marcus, M., et al. 2009b, ApJ, 701, 306

Elmegreen, D. M., Elmegreen, B. G., Ravindranath, S., & Coe, D. A. 2007, ApJ, 658, 763
Elmegreen, D. M., Elmegreen, B. G., Rubin, D. S., & Schaffer, M. A. 2005b, ApJ, 631, 85
Elmegreen, D. M., Elmegreen, B. G., Sánchez Almeida, J., et al. 2012, ApJ, 750, 95
Elmegreen, D. M., Elmegreen, B. G., Yau, A., et al. 2011, ApJ, 737, 32
Fischera, J., Dopita, M. A., & Sutherland, R. S. 2003, ApJ, 599, 21
Förster Schreiber, N. M., Genzel, R., Bouché, N., et al. 2009, ApJ, 706, 1364
Förster-Schreiber, N. M., Genzel, R., Lehnert, M. D., et al. 2006, ApJ, 645, 1062
Garland, C. A., Pisano, D. J., Williams, J. P., Guzmán, R., & Castander, F. J. 2004, ApJ, 615, 689
Garland, C. A., Pisano, D. J., Williams, J. P., et al. 2007, ApJ, 671, 310
Garn, T., & Best, P. N. 2010, MNRAS, 409, 421
Genzel, R., Burkert, A., Bouché, N., et al. 2008, ApJ, 687, 59
Genzel, R., Newman, S., Jones, T., et al. 2011, ApJ, 733, 101
Genzel, R., Tacconi, L. J., Eisenhauer, F., et al. 2006, Natur, 442, 786
Gil de Paz, A., Madore, B. F., & Pevunova, O. 2003, ApJS, 147, 29
Heckman, T. M., Hoopes, C. G., Seibert, M., et al. 2005, ApJL, 619, L35
Heidmann, J. 1987, in IAU Symp. 115, Star Forming Regions, ed. M. Peimbert & J. Jugaku (Dordrecht: Reidel), 599
Hibbard, J. E., & Vacca, W. D. 1997, AJ, 114, 1741
Hoffman, G. L., Brosch, N., Salpeter, E. E., & Carle, N. J. 2003, AJ, 126, 2774
Hoopes, C., Heckman, T. M., Salim, S., et al. 2007, ApJS, 173, 441
Hoyos, C., Guzmán, R., Díaz, A. I., Koo, D. C., & Bershady, M. A. 2007, AJ, 134, 2455
Kartaltepe, J. S., Dickinson, M., Alexander, D. M., et al. 2012, ApJ, 757, 23
Kaviraj, S., Cohen, S., Windhorst, R. A., et al. 2013, MNRAS, 429, L40
Kennicutt, R. C. 1998, ARA&A, 36, 189
Kniazev, A. Y., Pustilni, S. A., Ugryumov, A. V., & Pramsky, A. G. 2001, A&A, 371, 404
Law, D. R., Steidel, C. C., Erb, D. K., et al. 2009, ApJ, 697, 2057
Leitherer, C., Li, I.-H., Calzetti, D., & Heckman, T. M. 2002, ApJS, 140, 303
Madau, P. 1995, ApJ, 441, 18
Maehara, H., Hamabe, M., Bottinelli, L., et al. 1988, PASJ, 40, 47
Maiz-Apellaniz, J., Mas-Hesse, J. M., Muñoz-Tuñon, C., Vilchez, J. M., & Castaneda, H. O. 1998, A&A, 329, 409
Mannucci, F., Cresci, G., Maiolino, R., Marconi, A., & Gnerucci, A. 2010, MNRAS, 408, 2115
Mannucci, F., Cresci, G., Maiolino, R., et al. 2009, MNRAS, 398, 1915
McLure, R. J., Pearce, H. J., Dunlop, J. S., et al. 2013, MNRAS, 428, 1088
Melo, V. P., Muñoz-Tuñón, C., Maíz-Apellániz, J., & Tenorio-Tagle, G. 2005, ApJ, 619, 270
Miyauchi-Isobe, N., Maehara, H., & Nakajima, K. 2010, PNAOJ, 13, 9
Monreal Ibero, A., Colina, L., Arribas, S., & García-Marín, M. 2007, A&A, 472, 421
Morales-Luis, A. B., Sánchez Almeida, J., Aguerri, J. A. L., & Muñoz-Tuñón, C. 2011, ApJ, 743, 77
Newman, S. F., Genzel, R., Forster Schreiber, N. M., et al. 2013, ApJ, 767, 104
Noeske, K., Guseva, N., Frick, K., et al. 2000, A&A, 361, 33
Overzier, R., Heckman, T. M., Kauffmann, G., et al. 2008, ApJ, 677, 37
Overzier, R. A., Heckman, T. M., Schiminovich, D., et al. 2010, ApJ, 710, 979
Overzier, R. A., Heckman, T. M., Tremonti, C., et al. 2009, ApJ, 706, 203
Papaderos, P., Guseva, N. G., Izotov, Y. I., & Fricke, K. J. 2008, A&A, 491, 113
Petty, S. M., de Mello, D. F., Gallagher, J. S., III, et al. 2009, AJ, 138, 362
Puech, M., Hammer, F., Hopkins, P. F., et al. 2012, ApJ, 753, 128
Pustilnik, S. A., Brinks, E., Thuan, T. X., Lipovetsky, V. A., & Izotov, Y. I. 2001, AJ, 121, 1413
Putman, M. E., Bureau, M., Mould, J. R., Staveley-Smith, L., & Freeman, K. C. 1998, AJ, 115, 2345
Queyrel, J., Contini, T., Kissler-Patig, M., et al. 2012, A&A, 539, A93
Rafelski, M., Wolfe, A. M., Cooke, J., et al. 2009, ApJ, 703, 2033
Sánchez Almeida, J., Muñoz-Tuñón, C., Elmegreen, D. M., Elmegreen, B. G., & Méndez-Abreu, J. 2013, ApJ, 767, 74
Shapley, A. E. 2011, ARA&A, 49, 525
Sheth, K., Regan, M., Hinz, J. L., et al. 2010, PASP, 122, 1397
Stoughton, C., Lupton, R. H., Bernardi, M., et al. 2002, AJ, 123, 485
Tacconi, L. J., Neri, R., Genzel, R., et al. 2013, ApJ, 768, 74
Taylor, C. L., Thomas, D. L., Brinks, E., & Skillman, E. D. 1996, ApJS, 107, 143
Thuan, T. X., & Izotov, Y. I. 1997, ApJ, 489, 623
van Zee, L., Skillman, E. D., & Salzer, J. J. 1998a, AJ, 116, 1186
van Zee, L., Westpfahl, D., Haynes, M. P., & Salzer, J. J. 1998b, AJ, 115, 1000
Weiner, B. J., Willmer, C. N. A., Faber, S. M., et al. 2006, ApJ, 653, 1027
Wilcots, E. M., & Miller, B. W. 1998, AJ, 116, 2363
Wisnioski, E., Glazebrook, K., Blake, C., et al. 2011, MNRAS, 417, 2601
Wisnioski, E., Glazebrook, K., Blake, C., et al. 2012, MNRAS, 422, 3339